Fragmentation in the mechanical instability region

David H. Boal
Department of Physics, Simon Fraser University, Burnaby, British Columbia, Canada V5A 1S6

Alan L. Goodman
Department of Physics and Quantum Theory Group, Tulane University, New Orleans, Louisiana 70118
(Received 25 November 1985)

By means of a cascade model calculation, it is shown that medium mass fragment production in proton-induced reactions very likely proceeds via the breakup of the residual nuclear system rather than coalescence. The reaction trajectory of the excited nuclear system is found to enter the mechanical instability region with $S/A \sim 0.4$, well below the average S/A of 1.6–2.0 observed experimentally for heavy fragments in proton-induced reactions. We estimate the increase in entropy generated by passage through the mechanical instability region of nuclear matter by means of two simple models. The predicted final entropy is comparable to what is found experimentally.

I. INTRODUCTION

The NN interaction exhibits a short distance repulsion and a long distance attraction, which suggests that nuclear matter has a liquid-gas phase transition similar to that of a van der Waals fluid.[1–6] The critical temperature and density estimated[7–10] for the phase transition argue that it may be accessible experimentally. Indeed, analysis of two-particle correlation measurements for light fragments produced in intermediate energy heavy ion reactions shows[11,12] that the reaction region sizes and temperatures are in the phase transition region at freezeout. Of course, whether one can speak of a discrete phase transition for the finite and probably inhomogeneous systems found in these heavy ion reactions remains to be seen.

Historically, one of the first experimental measurements which invoked the phase transition idea for its description was the mass yield curve observed in high energy proton-induced fragmentation.[13–15] Unfortunately, there are several alternative descriptions[16–21] of the mass yield curves, not all of which require the existence of a phase transition. Further, that part of the phase diagram through which it is hypothesized the reaction region passes in these experiments is the critical region, where, in fact, discontinuities associated with the phase transition should vanish. In an effort to search for an experimental variable which may show a discontinuity at the phase transition, we will concentrate on the mechanical instability region at low entropy or temperature.

We begin our study of this region in Sec. II with the derivation of the properties of the phase diagram from a zero-range Skyrme-type interaction. Although the equation of state we have chosen is different from some used previously, it will be demonstrated that the properties of the mechanical instability region are similar, giving one some hope that the predictions are stable against changes in parametrization.

One of the difficulties of the experimental signatures presented thus far has been the presence of at least one free parameter and some license in choosing the temperatures and densities assumed to be applicable in the reaction under investigation. We choose to avoid these problems by performing a numerical simulation of the reaction trajectory involved by using a simplified Boltzmann-Uehling-Uhlenbeck (BUU) model for proton-induced fragmentation at intermediate energies. In Sec. III the model is presented, tested, and used to investigate the reaction conditions. Using this technique, it is demonstrated that coalescence and condensation contributions to medium mass fragment production in this reaction are minimal and that fragmentation most likely involves the breakup of the cool residual nucleus.

The possibility that entropy can be used as a phase transition signature is examined in Sec. IV. The BUU simulation is used to predict the entropy in the absence of mechanical breakup or evaporation, and it is found to be small. Two simple models are then used to estimate the entropy production at the phase transition and it is shown that the entropy roughly triples during fragmentation. This prediction is then tested against experiment by means of an extended chemical equilibrium model which includes a prescription for including heavy fragments. Our conclusions are summarized in Sec. V.

II. EQUATION OF STATE

Our equation of state[22] is derived from a zero-range Skyrme-type interaction,

$$V_{12}=\left[-t_0+\frac{t_3}{6}\rho\right]\delta(\mathbf{r}_1-\mathbf{r}_2)\,, \tag{2.1}$$

where ρ is the density at $(\mathbf{r}_1+\mathbf{r}_2)/2$. The single nucleon energies in nuclear matter are given by the finite-temperature Hartree-Fock approximation

$$\epsilon_k=\frac{\hbar^2k^2}{2m}+\epsilon_0\,, \tag{2.2}$$

where the interaction energy ϵ_0 is

$$\epsilon_0=-2a_0\rho+3a_3\rho^2\,, \tag{2.3}$$

and $a_0=\frac{3}{8}t_0$, $a_3=\frac{1}{16}t_3$.

The occupation probability for a level with energy ϵ_k is given by the Fermi-Dirac distribution

$$f(\epsilon_k)=\frac{1}{e^{(\epsilon_k-\mu)/T}+1} . \tag{2.4}$$

The chemical potential μ is determined by the constraint that the sum of the occupation probabilities is equal to the number of nucleons A; that is,

$$A=g_{S,I}\sum_{\mathbf{k}} f(\epsilon_k) , \tag{2.5}$$

where the spin-isospin degeneracy factor $g_{S,I}$ is 4. It is assumed that $N=Z$. This sum is approximated by the integral

$$A=\int_{\epsilon_0}^{\infty} d\epsilon\, \mathscr{D}(\epsilon) f(\epsilon) , \tag{2.6}$$

where the density of states is

$$\mathscr{D}(\epsilon)=g_{S,I}\left[\frac{V}{4\pi^2}\right]\left[\frac{2m}{\hbar^2}\right]^{3/2}(\epsilon-\epsilon_0)^{1/2} , \tag{2.7}$$

and the volume V is A/ρ. The equation of state $P(\rho,T)$ is given by

$$P=P_{\text{kin}}+P_{\text{int}} , \tag{2.8}$$

where the kinetic pressure and the interaction pressure are

$$P_{\text{kin}}=\frac{T}{V}\ln z=-\frac{T}{V}\int_{\epsilon_0}^{\infty} d\epsilon\, \mathscr{D}(\epsilon)\ln[1-f(\epsilon)] , \tag{2.9}$$

$$P_{\text{int}}=-a_0\rho^2+2a_3\rho^3 , \tag{2.10}$$

and z is the grand partition function for independent fermions. The energy is

$$E=E_{\text{kin}}+E_{\text{int}} , \tag{2.11}$$

where

$$E_{\text{kin}}=\sum_{\mathbf{k}}\frac{\hbar^2k^2}{2m}=\sum_{\mathbf{k}}(\epsilon_k-\epsilon_0)$$

$$=\int_{\epsilon_0}^{\infty} d\epsilon\, \mathscr{D}(\epsilon) f(\epsilon)(\epsilon-\epsilon_0) , \tag{2.12}$$

$$E_{\text{int}}=(-a_0\rho+a_3\rho^2)A . \tag{2.13}$$

The entropy is

$$S=-\int_{\epsilon_0}^{\infty} d\epsilon\, \mathscr{D}(\epsilon)\{f(\epsilon)\ln f(\epsilon)$$

$$+[1-f(\epsilon)]\ln[1-f(\epsilon)]\} . \tag{2.14}$$

It is instructive to separate the chemical potential into components

$$\mu=\mu_{\text{kin}}+\mu_{\text{int}} , \tag{2.15}$$

where $\mu_{\text{int}}=\epsilon_0$. As is well known, when the temperature is zero, the integrals above can be evaluated analytically, with the result that

$$\mu_{\text{kin}}=\epsilon_F=(\hbar^2/2m)(\tfrac{3}{2}\pi^2\rho)^{2/3} , \tag{2.16}$$

$$P_{\text{kin}}=\tfrac{2}{5}\rho\epsilon_F , \tag{2.17}$$

$$E_{\text{kin}}=\tfrac{3}{5}\epsilon_F A , \tag{2.18}$$

where ϵ_F is the Fermi energy.

The constants in the interaction are chosen as $t_0=782$ MeV fm^3 and $t_3=10\,666$ MeV fm^6. Then the ground state properties are $\rho_0=0.15$ fm^{-3}, $E_0/A=-7.8$ MeV, and the compressibility $K=229$ MeV. These numbers simulate the properties of a finite nucleus.

For finite temperatures, the integrals are evaluated numerically with 3000 bins. The upper limit of integration is replaced by ϵ_{max}, where

$$\epsilon_{\text{max}}=\epsilon_F+\epsilon_0+15T . \tag{2.19}$$

The equation of state $P(\rho,T)$ is shown in Fig. 1. There is a critical point at $T_c=15.3$ MeV and $\rho_c/\rho_0=0.415$. The entropy per nucleon at the critical point is 2.5. Other authors, using different equations of state, also find $S_c/A=2.5$. For $T<T_c$, Fig. 1 displays the characteristic van der Waals behavior, which typifies a liquid-gas phase transition.

The phase diagram in Fig. 2 is constructed from the equation of state $P(\rho,T)$. The Maxwell construction is used to define the liquid-gas coexistence (LGC) curve. The constraint $(\partial P/\partial\rho)_T=0$ determines the isothermal spinodal (ITS) curve, whereas the constraint $(\partial P/\partial\rho)_S=0$ defines the isentropic spinodal (IES) curve. The stable liquid and gas phases are to the right and left, respectively, of the LGC curve. The metastable phases lie between the LGC and ITS curves. If nuclear matter ex-

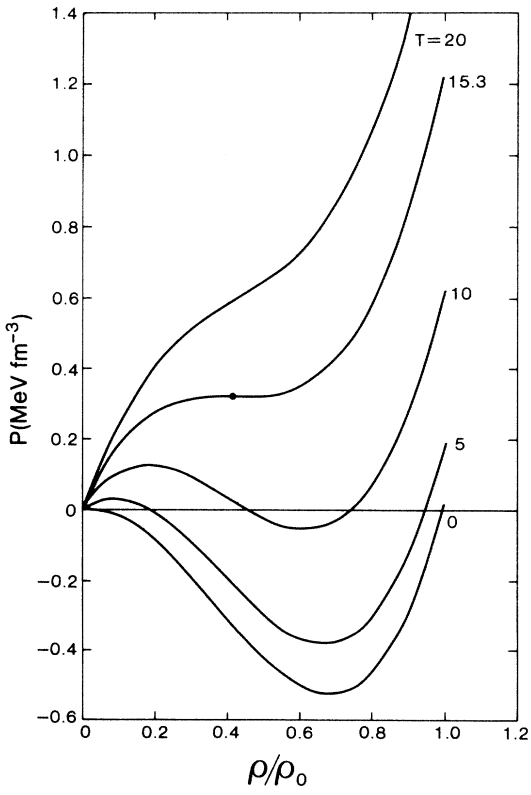

FIG. 1. Equation of state found from the zero range Skyrme-type interaction described in the text. The temperatures are shown in MeV for each isotherm.

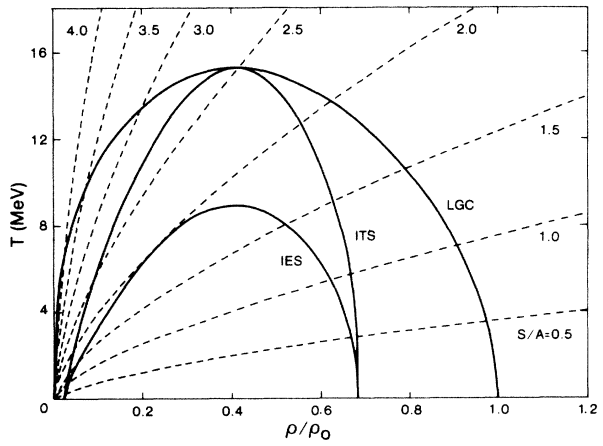

FIG. 2. Phase diagram for nuclear matter associated with Fig. 1. The dashed curves are isentropes with the value of S/A indicated for each. Shown as well are the liquid-gas coexistence boundary (LGC), isothermal spinodal (ITS), and isentropic spinodal (IES).

pands slowly at constant temperature, then the mechanically unstable phase is within the ITS curve. However, if the expansion occurs at constant entropy, then the mechanically unstable region is inside the IES curve. Observe that the peak in the IES is far below that of the ITS. Isentropes with S/A ranging from 0.5 to 4.0 are the dashed lines in Fig. 2. The state of maximum entropy on the IES curve has $S/A=1.98$. If adiabatically expanding matter has $S/A>1.98$, then it will not enter the region of mechanical instability.

In summary, we find that even though we have used a different equation of state than many used previously, the properties of nuclear matter in the phase transition region are found to be similar.

III. NUMERICAL SIMULATION OF THE REACTION

To investigate the reaction path followed in an intermediate energy proton-induced reaction, we make use of a simplified Boltzmann-Uehling-Uhlenbeck model.[23–25] (For other approaches to the time evolution of proton- and heavy-ion-induced reactions, see Refs. 26–29.) Target nucleons are placed in a spatially fixed spherical step function potential well and their collisions both with each other and with the projectile (as well as their elastic collisions with the wall of the potential well) are followed using classical mechanics. The justification for using a spatially fixed well is that (i) we are principally interested in the thermalization process and so the reaction is followed for less than 10^{-22} sec, of the order of the transit time of the projectile. Hence (ii) for the $p+(A=100)$ reaction considered here, even when the projectile is completely absorbed by the target, the velocity of the target is so slow that it has moved much less than a fermi during this time frame.

A simplified approach is also taken to Pauli blocking. As will be emphasized below, unlike a heavy ion reaction, the nucleon multiplicity in an intermediate energy proton-induced reaction is observed (and predicted here) to be very low.[26] Hence, the occupancy of the target energy levels remains near unity during the projectile's transit. Our prescription for Pauli blocking is that any collision which results in a nucleon being scattered into a state below the Fermi surface is blocked. These two simplifications only limit the usefulness of the code at long times ($>10^{-21}$ sec).

The nucleon-nucleon cross sections are taken to have the energy dependence

$$\sigma_{pp}=\sigma_{nn}=13.2\lambda\!\!\!^{-2}\,,\qquad \sigma_{pn}=42.5\lambda\!\!\!^{-2} \tag{3.1}$$

at low energies and

$$\sigma_{pp}=\sigma_{nn}=2.2\ \text{fm}^2\,,\qquad \sigma_{pn}=3.4\ \text{fm}^2 \tag{3.2}$$

at high energies, where $\lambda\!\!\!^{-}=\hbar/p$ and p is the laboratory momentum. Half of the pn scatterings are taken to result in charge exchange. The cross sections are assumed to be isotropic in the center of mass frame. Since pion production is not important at these energies for the quantities in which we are interested, it is neglected.

We first examine a few of the predictions of the code which can be compared to experiment. Shown in Fig. 3 is the distribution in momentum space of the nucleons which have been knocked out of the target. Bound nucleons are not included in this plot. Illustrated is an impact parameter averaged 300 MeV $p+(A=100)$ collision. The density has units of the number of particles per (50 MeV/c)^3 bin. The momentum distribution has been sam-

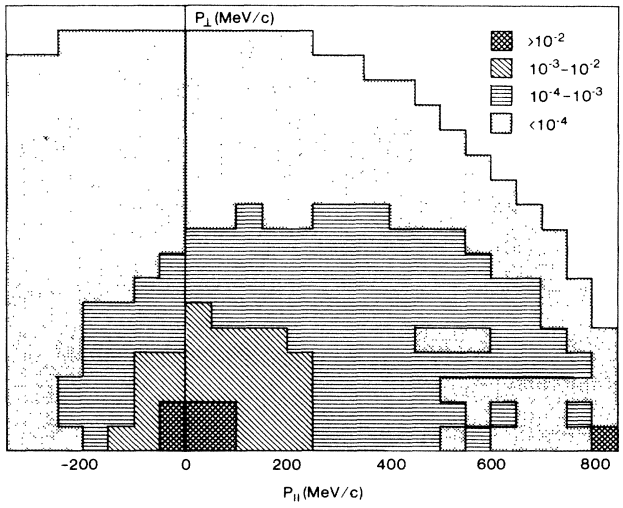

FIG. 3. Model prediction for the free particle momentum space density in an impact parameter averaged 300 MeV $p+(N=Z=50)$ collision. The density is given in units of nucleons per (50 MeV/c)^3. Nucleons bound in the nucleus are not included in this plot. The distribution was sampled at 8×10^{-23} sec after the projectile had entered the nucleus.

pled at 8×10^{-23} sec. One sees that the familiar semicircular shape (for contours of constant momentum density) found in the analysis[26] of the data is reproduced by the simulation, as is the appearance of a quasielastic peak. Further, the origin of the semicircles on the $p_{||}$ axis increases with decreasing density, as is observed experimentally.

Even though the model has predicted a thermal (i.e., exponential) spectrum for the emitted nucleons, one should not assume that there is, in fact, thermal equilibrium. By equilibrium, we mean whether the time between nucleon collisions is short compared to the expansion time of the nucleon gas. To answer this question, it is instructive to examine the spatial densities associated with the free nucleons knocked out of the target. These are shown in Fig. 4 for a central 300 MeV p+($Z=N=50$) collision. The top part of the figure shows the spatial densities 4×10^{-23} sec after the projectile has entered the target (from the left). At this time, the projectile is about half way through the target. The bottom part of the figure shows the densities after transit; the probability density associated with the projectile appears on the far right. Clearly, the densities at this point are very low, typically $\frac{1}{20}\rho_0$. Such low densities imply a long collision time, and the system is out of thermal equilibrium. It is also worth mentioning that the nucleon gas is far from being spatially uniform.

We expect, then, that the collision rate is low in proton-induced reactions. This is illustrated in Fig. 5, again for central 300 MeV p+($Z=N=50$) collisions. Scatterings which involve only nucleons below the Fermi surface are omitted in this figure. One can see that the collision rate climbs as the projectile passes through the target, but drops rapidly as it leaves. Further, even at the peak, many of the collisions are Pauli-blocked, as is indicated by the shaded region. Hence, the reaction appears to be more like sequential scattering of the projectile than thermal equilibrium in a nucleon gas.

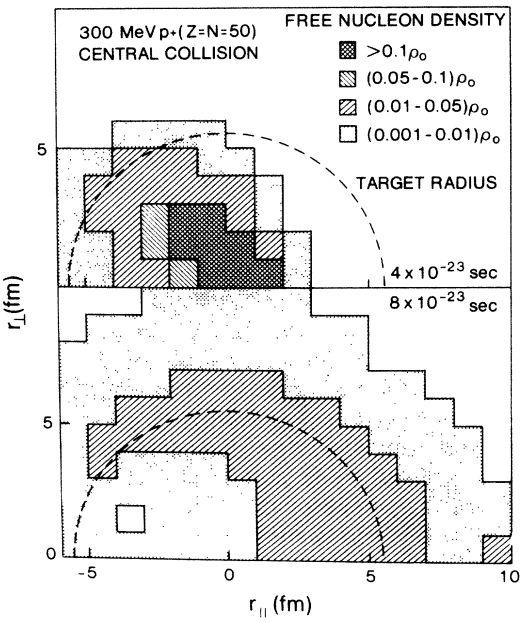

FIG. 4. Model prediction for spatial densities (in units of ρ_0) in a central 300 MeV p+($N=Z=50$) collision. The densities are shown 4×10^{-23} and 8×10^{-23} sec after the projectile has entered from the left. As in Fig. 3, only those nucleons with enough energy to escape the target are included.

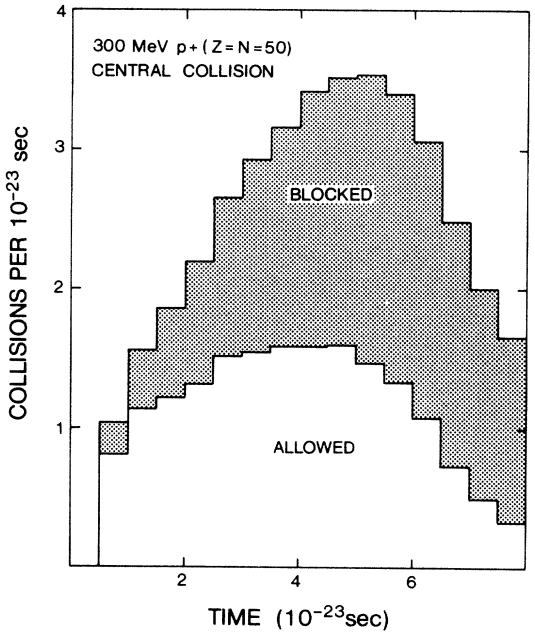

FIG. 5. Time dependence of the NN collision rate predicted for a central 300 MeV p+($N=Z=50$) reaction. Collisions solely among target nucleons in the Fermi sea are neglected. Those collisions which are Pauli-blocked are indicated by the shaded region.

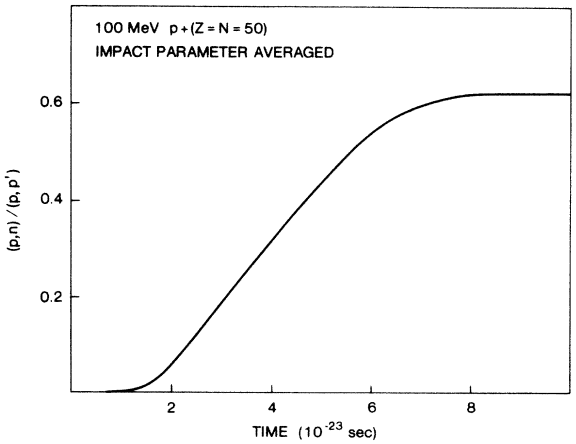

FIG. 6. Time dependence of the ratio of unbound neutrons to protons predicted for the 100 MeV p+($N=Z=50$) reaction with impact parameter averaging. Chemical equilibrium is not achieved.

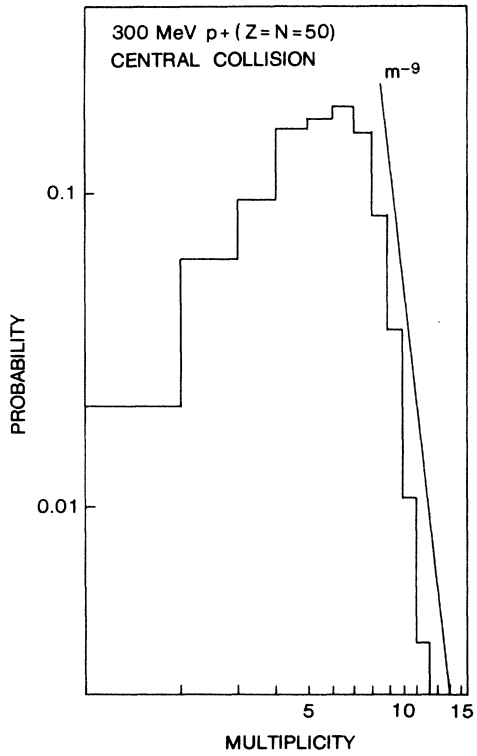

FIG. 7. Nucleon multiplicity distribution predicted for a 300 MeV p+($N=Z=50$) central collision. The multiplicity drops very steeply above six. For peripheral collisions, the multiplicities are even lower.

One already knows from the experimentally measured[30] (p,n)/(p,p') ratio that chemical equilibrium among the nucleons is also not established.[31] This ratio, after unfolding N/Z effects associated with the target, is typically found to be $\sim\frac{1}{2}$, far from unity as expected at chemical equilibrium. The model predicts a similar value, as can be seen from Fig. 6.

In summary, the reason for the low collision rate is the low multiplicity and Pauli blocking. Is it possible that a subset of the collisions actually has a high enough nucleon multiplicity to achieve thermal and chemical equilibrium? The model predicts that this is unlikely. Shown in Fig. 7 is the multiplicity distribution predicted for central collisions in the 300 MeV p+($A=100$) reaction. One can see that, even for central collisions, the nucleon multiplicity falls off very rapidly above 6. For peripheral collisions, of course, the multiplicity will be even lower.

IV. FRAGMENTATION

In the preceding section we concentrated on developing a numerical simulation that described intermediate energy proton-induced reactions. We now wish to use that simulation to determine a scenario for fragment formation. Several potential contributing mechanisms for fragmentation in heavy-ion- and proton-induced reactions have been proposed, and the simulation can be used to help fix the limits of their applicability here.

One possible contribution is from the condensation [or coalescence (Refs. 32 and 33)] of the nucleon gas produced in the reaction. However, the low multiplicity of this gas suggests that outside of perhaps very light fragments, few composites could be formed. In particular, if one examines the multiplicity distribution for $m>6$, one sees that even for a central collision the dropoff is very rapid, having a power law dependence of m^{-9}. In contrast, the yield of medium mass fragments falls much more slow,[34] like m^{-3} or m^{-4}. Hence, there are unlikely to be enough nucleons free to condense into mass 10—20 fragments.

The model shows that nucleon and medium mass fragment emission very likely have different origins in this reaction. Hence, information derived from mass yield curves must be handled with some care. For example, a proposal[35] has been made in heavy ion reactions that the difference between the entropies extracted from very light versus medium mass fragments may be attributable to the liquid-gas phase transition. Such a difference in entropies is also observed in proton-induced reactions. Here, however, we find that nucleons and light mass fragments will have a strong contribution from simple knockout[36] (particularly once impact parameter averaging is taken into account), hence increasing their apparent entropy with respect to medium mass fragments. This knockout contribution, rather than the phase transition, is probably the origin of the entropy difference here. Of course, if one could reliably subtract the knockout contribution, one might still be left with a discrepancy, but our calculations are not yet accurate enough to do that.

Our conclusion, then, is that the most likely source of fragmentation is the breakup of the residual system.[17] One could imagine that this might proceed through the mechanical instability region[6] if the excitation energy is high enough, or through the more conventional evaporation mechanism at lower excitation energy.[37]

The simulation can be used to determine whether the mechanical instability region can be reached. It is straightforward to calculate the entropy in these simulations via a numerical integration of Eq. (2.14). We calculate only the entropy of the residual nucleus, not the system as a whole. This simplifies the integration of Eq. (2.14): The spatial volume integral is trivial since the nucleons are spread uniformly throughout the target. The distributions $f(\epsilon)$ are determined by averaging over many events at a given impact parameter. Because of the finite number of events, there will be some fluctuation in $f(\epsilon)$ about its mean for a given energy bin. This, in turn, generates what might be called numerical entropy. One can suppress these fluctuations by making the size of the energy bins larger, but again numerical entropy will be produced when $f(\epsilon)$ changes too rapidly with energy (such as it does near the Fermi energy) resulting in the average $f(\epsilon)$ deviating too far from the real distribution. In any event, we choose a sufficient number of events to keep the numerical specific entropy to less than 0.1. To find an excitation energy E^* in the model the energies of the nucleons in the excited residual nucleus are compared to the energies of the nucleons in their ground state.

The locus of E^*/A vs S/A predicted for a central collision at two different bombarding energies (for which ex-

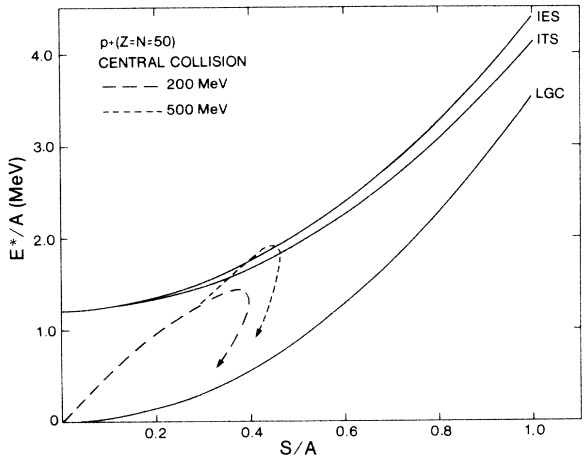

FIG. 8. Isothermal spinodal (ITS), isentropic spinodal (IES), and liquid-gas coexistence (LGC) curve shown as a function of excitation energy and entropy per nucleon. The reaction trajectories for the excited nuclear system predicted by the cascade model for 200 and 500 MeV $p+(N=Z=50)$ central collisions are shown by the dashed lines.

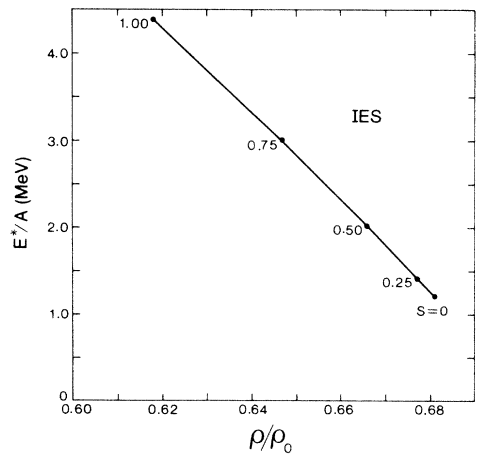

FIG. 9. Excitation energy per nucleon as a function of density along the isentropic spinodal found from the equation of state. Sample values of the specific entropy are indicated on the curve.

perimental data are available) is shown in Fig. 8. The system moves into the metastable region easily and just reaches the unstable region delimited by the isentropic spinodal curve. Most, but not all, impact parameters allow the trajectory to pass reasonably close to the unstable region. Because we are restricting our attention to the breakup of the target nucleus [in evaluating (2.14)] we find that the entropy increases as nucleons are knocked into their excited states, and then decreases as they "evaporate" and the residual nucleus returns to its ground state. If the total entropy were plotted in Fig. 8 instead of that of the residual system, it would tend to a constant rather than returning to zero.

The actual test of passage through the phase transition region is the calculation of the increase in entropy. First, from Fig. 8 we will take the point at which the system enters the mechanical instability region to have $S/A=0.4$. The corresponding excitation energy is 1.5 to 2 MeV per nucleon. As can be seen from Fig. 9, the density at the mechanical instability is about $\frac{2}{3}\rho_0$.

There will be several contributions to the entropy after fragmentation: entropy associated with the motion of the fragments themselves, entropy associated with their surfaces at finite temperature, and entropy associated with the internal motion of the nucleons. To evaluate these, a prediction for the fragment mass distribution is required. (For further work on this problem, see Refs. 37–42.) Since the equation of state contains no reference to surfaces, we must make further assumptions. We present two calculations in the subsections which follow.

A. Fluid model

We first obtain an estimate of the increase in bulk entropy for our equation of state by following a prescription suggested by Lopez and Siemens.[43] (See also Ref. 35.) During the fragmentation they assumed that the energy density and the number density are invariant, so that

$$E=\alpha E_g+(1-\alpha)E_l\ , \tag{4.1}$$

$$\frac{1}{\rho}=\frac{\alpha}{\rho_g}+\frac{(1-\alpha)}{\rho_l}\ . \tag{4.2}$$

The intersection of the appropriate isentrope with the IES curve determines E and ρ, as well as an initial temperature T_i. The gas mass fraction is α. If the final temperature of the mixture is T_f, then the Maxwell construction determines the properties of the coexisting liquid and gas phases, i.e., $\rho_l,\rho_g,E_l,E_g,S_l,S_g$. The two constraints, (4.1) and (4.2), are satisfied by numerically searching for the appropriate values of the two free parameters α and T_f. The volume entropy of the stable mixture is

$$S_f=\alpha S_g+(1-\alpha)S_l\ . \tag{4.3}$$

Figure 10 shows the final entropy S_f and the change in entropy $\Delta S=S_f-S_i$ vs the initial entropy S_i. Figure 11 depicts the initial temperature T_i and the final temperature T_f vs the initial entropy S_i. These figures resemble those of Lopez and Siemens, even though our equations of state are different. For an initial entropy of 0.4, the predicted change in entropy at the IES is 0.3.

Without a prediction for the mass distribution, we can only estimate the surface contribution. In Ref. 44, the surface entropy per unit area ($\equiv\sigma$) for a $Z=N$ surface is calculated to be 6×10^{-2} fm^{-2} at $T=5$ MeV (similar to the parametrization adopted in Ref. 22). For fragments in the mass 5–15 range, this calculation liberally could be interpreted as implying that $\Delta S/A$ from the surfaces is of the order 0.6–0.4. However, in the Fisher droplet model[45] there is a second contribution from the closing of the surfaces which will partially cancel this. If one were to calculate this contribution to S/A of the whole system of nearly 100 nucleons, the result would be substantially

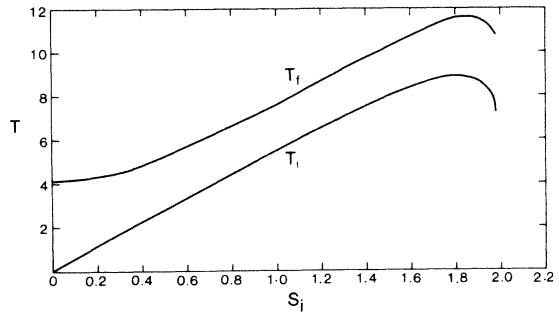

FIG. 10. Initial and final temperature at the isentropic spinodal shown as a function of initial entropy.

smaller.

The contribution of the kinetic motion of the nuclear droplets (not the nucleon gas) is found to be of a similar magnitude. Since the multiplicity of medium mass droplets is not large (experimentally), one can use the Sackur-Tetrode formula for the entropy per droplet, s (not per nucleon)

$$s=-\frac{\mu}{T}+2.5\ , \tag{4.4}$$

where μ is the chemical potential associated with the droplet. Since μ/T is negative, then for mass (5—15) droplets S/A must be at least 0.5—0.16.

In Fisher's droplet model, the bulk entropy, surface entropy, and kinetic entropy of the droplets are additive. Consequently, we would expect from these estimates that the increase in entropy per nucleon for medium mass fragments generated at the IES should be in the range 0.5—2.

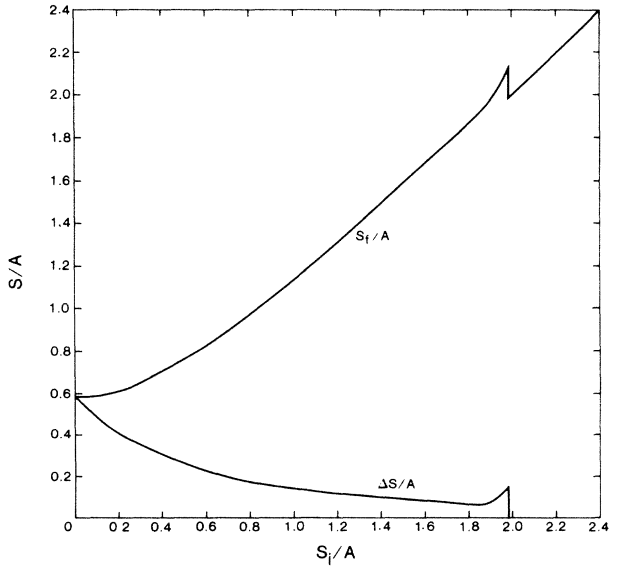

FIG. 11. Change in entropy at the isentropic spinodal shown as a function of initial entropy.

B. Chemical equilibrium model

A model which allows us to make a definitive prediction is to assume chemical equilibrium among all the products at breakup. Two parameters will be involved, T and μ, and these can be fixed by imposing the same constraints as were used in the preceding section to determine the bulk entropy, namely, that nucleon number density and energy density be conserved at the IES.

Because very heavy fragments must be included in our entropy calculation, the chemical equilibrium model used previously[46] in analyzing mass yield data must be extended. The details of our calculation are as follows:

(i) For nuclei with mass less than 17, the first 15 states are explicitly included for each nuclide. This energy cut was used since the temperatures found from the particle yields are typically 3 MeV or less.

(ii) For masses greater than 16, a fit was made to the density of states, including their spin. It was found that the following parametrization provided an approximate fit to the densities:

$$D(\epsilon)=\alpha\exp(\beta\epsilon)\ , \tag{4.5}$$

where

$$\begin{aligned}\alpha&=0.204A+1.20\ \text{MeV}^{-1}\ ,\\ \beta&=0.0057A+0.603\ \text{MeV}^{-1}\ .\end{aligned} \tag{4.6}$$

These formulas were obtained by averaging over a wide range of A. Specific nuclei may have densities very different from what (4.6) would predict. Hence while the formulas may be useful for estimating the summed yield and associated entropy of heavy fragments, they will not be valid for specific nuclei or narrow mass ranges. The occupation distributions for each state are then determined by μ_N and T, where μ_N is the chemical potential per nucleon, defined such that

$$f(\epsilon)\simeq\exp[(A\mu_N-\Delta-E)/T]\ , \tag{4.7}$$

where Δ is the mass excess. One could then integrate Eq. (2.14) to obtain the entropy associated with each level. In fact, this is unnecessary since the f's turn out to be sufficiently small that Eq. (2.14) can be replaced by the approximation

$$S=-(A\mu_N-\Delta)/T+\tfrac{5}{2}\ . \tag{4.8}$$

To the accuracy quoted here, this replacement is even valid for nucleons. The states are then summed over with their appropriate occupancy (up to mass 100) to obtain S/A for the entire system. For $S/A=0.4$ and $E^*/A=1.75$ MeV initially, the model yields $\mu_N/T=-1.1$, $T=3.4$ MeV, and a final S/A of 1.65. This increase in entropy is in the range expected on the basis of the fluid model calculation.

The chemical equilibrium code can also be used for experimental analysis. The only extra ingredient is the inclusion of the decay chains for nuclei of mass 16 or less. The decay channels were taken from Ref. 47 for those states included in the code, where available. One could in-

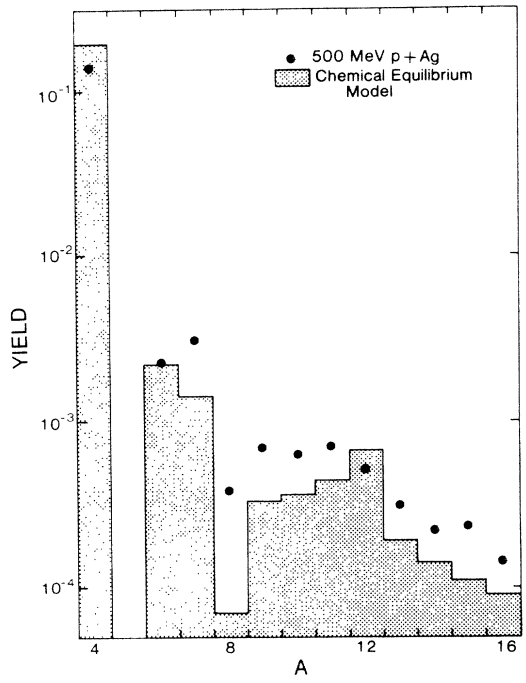

FIG. 12. Mass yield curve predicted by the chemical equilibrium model for $\mu_N = -1.12$ MeV, $T = 2.8$ MeV, and $V = 3500$ fm^3. The yields of medium mass fragments found in the 500 MeV p + Ag reaction are shown for comparison.

clude a prescription for decays of states at excitation energy, as has been suggested[48] for the analysis of heavy ion reactions, but again, this is not likely to make a significant difference for the low temperatures found here. Analyzing the 500 MeV p + Ag medium mass fragment yields, we find $\mu_N/T = -1.12$, $T = 2.8$ MeV, and, from the absolute normalization, $V = 3500$ fm^3. This latter quantity corresponds to a freezeout density of $\sim \frac{1}{5}\rho_0$, although the error on the volume is considerable (e.g., a volume of 2600 fm^3 gives only a slightly worse fit). The specific entropy is calculated to be 1.6, in agreement with the prediction. The entropy extracted here from the data is lower than that found previously because of the presence of the higher masses in the code. The overall form of the mass yield for these values of T and μ is shown in Fig. 12.

V. SUMMARY

Using a simplified Boltzmann-Uehling-Uhlenbeck model, we have performed a computer simulation of an intermediate energy proton-induced reaction. The simulation confirms the experimental observation of low nucleon multiplicity and shows that the nucleon emission involves multiple scatterings of the projectile but few rescatterings of the secondaries. Medium mass fragment emission[49] must then arise from, for example, statistical emission or mechanical breakup of the residual system. Taking the latter approach, we have mapped out the mechanical instability region of the phase diagram generated from a zero-range Skyrme-type interaction. The numerical simulation indicates that the isentropic spinodal is reached by the residual system. Two simple models are used to calculate the increase in the entropy at the isentropic spinodal. The first, using simple fluid arguments, gives only a range of values, but the second, assuming chemical equilibrium for an ideal gas, predicts an increase in the entropy which is in accord with what is observed experimentally.

ACKNOWLEDGMENTS

We wish to thank S. Das Gupta (McGill), B. Jennings (TRIUMF), and P. J. Siemens (Texas A & M) for many useful discussions. We are also grateful to both the Natural Sciences and Engineering Research Council of Canada and the U.S. National Science Foundation for financial support.

[1]G. Sauer, H. Chandra, and U. Mosel, Nucl. Phys. **A264**, 221 (1976).
[2]D. Q. Lamb, J. M. Lattimer, C. J. Pethick, and D. G. Ravenhall, Phys. Rev. Lett. **41**, 1623 (1978).
[3]P. Danielewicz, Nucl. Phys. **A314**, 465 (1979).
[4]H. Schulz, L. Münchow, G. Röpke, and M. Schmidt, Phys. Lett. **119B**, 12 (1982).
[5]M. W. Curtin, H. Toki, and D. K. Scott, Phys. Lett. **123B**, 289 (1983).
[6]G. Bertsch and P. J. Siemens, Phys. Lett. **126B**, 9 (1983).
[7]H. R. Jaqaman, A. Z. Mekjian, and L. Zamick, Phys. Rev. C **29**, 2067 (1984).
[8]S. Levit and P. Bonche, Nucl. Phys. **A437**, 426 (1985).
[9]I. Lovas and Gy. Wolf, Central Research Institute (Budapest) Report KFKI-1984-24, 1984.
[10]H. Reinhardt and H. Schulz, Nucl. Phys. **A432**, 630 (1985).
[11]C. B. Chitwood *et al.*, Phys. Rev. Lett. **54**, 302 (1985).
[12]D. H. Boal and J. C. Shillcock, Phys. Rev. C **33**, 549 (1986).
[13]J. E. Finn *et al.*, Phys. Rev. Lett. **49**, 1321 (1982).
[14]R. W. Minich *et al.*, Phys. Lett. **118B**, 458 (1982).
[15]For a general review of these reactions, see D. H. Boal, in *Advances in Nuclear Physics*, edited by J. W. Negele and E. Vogt (Plenum, New York, 1985), Vol. 15, pp. 85–214.
[16]D. H. Boal, Phys. Rev. C **28**, 2568 (1983).
[17]J. Aichelin, J. Hüfner, and R. Ibarra, Phys. Rev. C **30**, 107 (1984).
[18]D. H. E. Gross, L. Satpathy, Meng Ta-Chung, and M. Satpathy, Z. Phys. A **309**, 41 (1982).
[19]Sa Ban-Hao and D. H. E. Gross, Nucl. Phys. **A437**, 643 (1985).
[20]W. Bauer, D. R. Dean, U. Mosel, and U. Post, Phys. Lett. **150B**, 53 (1985).
[21]X. Campi, J. Desbois, and E. Lipparini, Phys. Lett. **142B**, 8 (1984); X. Campi and J. Desbois, Proceedings of the 7th High Energy Heavy Ion Study, Gesellschaft für Schwerionenforschung Report GSI-85-10, 1985, p. 707.
[22]For a review, see A. L. Goodman, J. I. Kapusta, and A. Z. Mekjian, Phys. Rev. C **30**, 851 (1984).
[23]G. Bertsch, H. Kruse, and S. Das Gupta, Phys. Rev. C **29**, 673 (1984).

[24]H. Kruse *et al.*, Phys. Rev. C **31**, 1770 (1985).
[25]J. Aichelin and G. Bertsch, Phys. Rev. C **31**, 1730 (1985).
[26]D. H. Boal and J. H. Reid, Phys. Rev. C **29**, 973 (1984).
[27]H. Stocker *et al.*, Nucl. Phys. **A400**, 63c (1983).
[28]J. Cugnon (unpublished).
[29]H. S. Köhler and B. S. Nilsson, Nucl. Phys. **A417**, 541 (1984).
[30]B. D. Anderson *et al.*, Phys. Rev. Lett. **46**, 226 (1981).
[31]D. H. Boal, Phys. Rev. C **29**, 967 (1984).
[32]S. T. Butler and C. A. Pearson, Phys. Rev. Lett. **7**, 69 (1961).
[33]A. Schwarzschild and C. Zupancic, Phys. Rev. **129**, 854 (1963).
[34]R. E. L. Green, R. G. Korteling, and K. P. Jackson, Phys. Rev. C **29**, 1806 (1984).
[35]L. P. Csernai, Phys. Rev. Lett. **54**, 639 (1985).
[36]R. E. L. Green, D. H. Boal, R. Helmer, K. P. Jackson, and R. G. Korteling, Nucl. Phys. **A405**, 463 (1983).
[37]This question has been addressed in heavy ion reactions by J. P. Bondorf, R. Donangelo, H. Schulz, and K. Sneppen, Niels Bohr Institute Report NBI-85-14, 1985. See also H. Schulz, B. Kämpfer, H. W. Barz, G. Röpke, and J. P. Bondorf, Phys. Lett. **147B**, 17 (1984).
[38]B. Strack and J. Knoll, Z. Phys. A **315**, 249 (1984).
[39]J. Knoll and B. Strack, Phys. Lett. **149B**, 45 (1984).
[40]A. Vincentini, G. Jacucci, and V. R. Pandharipande, Phys. Rev. C **31**, 1783 (1985).
[41]C. Gale and S. Das Gupta, Phys. Lett. (in press).
[42]G. E. Beauvais, D. H. Boal, and J. Wong (unpublished).
[43]J. A. Lopez and P. J. Siemens, Nucl. Phys. **A431**, 728 (1984).
[44]D. G. Ravenhall, C. J. Pethick, and J. M. Lattimer, Nucl. Phys. **A407**, 571 (1983).
[45]M. E. Fisher, in *Critical Phenomena,* Proceedings of the International School of Physics, "Enrico Fermi," Course LI, edited by M. S. Green (Academic, New York, 1971), p. 1.
[46]B. V. Jacak, H. Stöcker, and G. Westfall, Phys. Rev. C **29**, 1744 (1984). See also J. Randrup and G. Fai, Phys. Lett. **115B**, 281 (1982).
[47]*Table of Isotopes,* 7th ed., edited by C. M. Lederer and V. S. Shirley (Wiley, New York, 1978).
[48]D. Hahn and H. Stöcker (private communication).
[49]W. A. Friedman and W. G. Lynch, Phys. Rev. C **28**, 16 (1983).

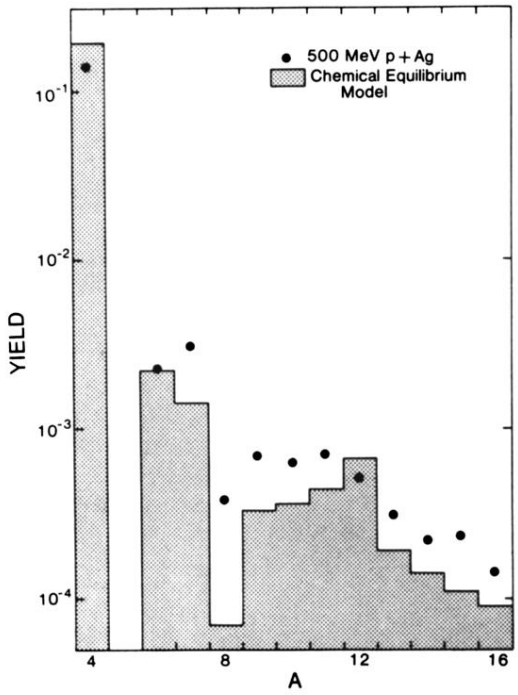

FIG. 12. Mass yield curve predicted by the chemical equilibrium model for $\mu_N = -1.12$ MeV, $T = 2.8$ MeV, and $V = 3500$ fm^3. The yields of medium mass fragments found in the 500 MeV p + Ag reaction are shown for comparison.

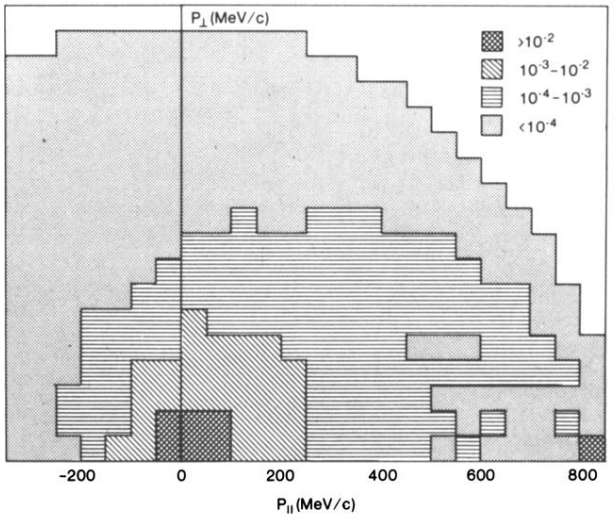

FIG. 3. Model prediction for the free particle momentum space density in an impact parameter averaged 300 MeV $p+(N=Z=50)$ collision. The density is given in units of nucleons per $(50\ \mathrm{MeV}/c)^3$. Nucleons bound in the nucleus are not included in this plot. The distribution was sampled at 8×10^{-23} sec after the projectile had entered the nucleus.

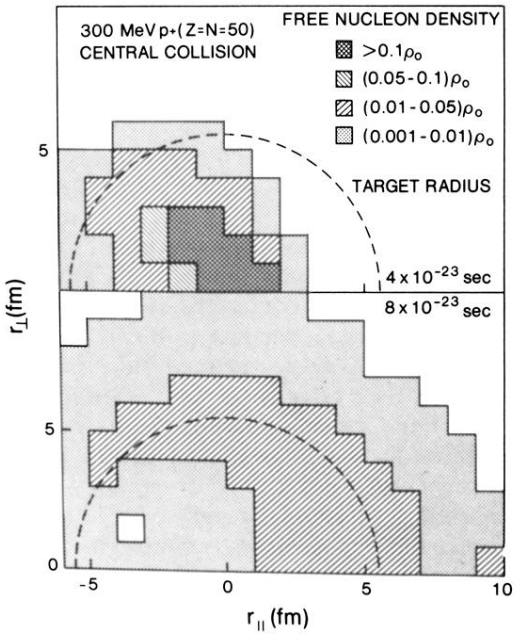

FIG. 4. Model prediction for spatial densities (in units of ρ_0) in a central 300 MeV p+($N=Z=50$) collision. The densities are shown 4×10^{-23} and 8×10^{-23} sec after the projectile has entered from the left. As in Fig. 3, only those nucleons with enough energy to escape the target are included.

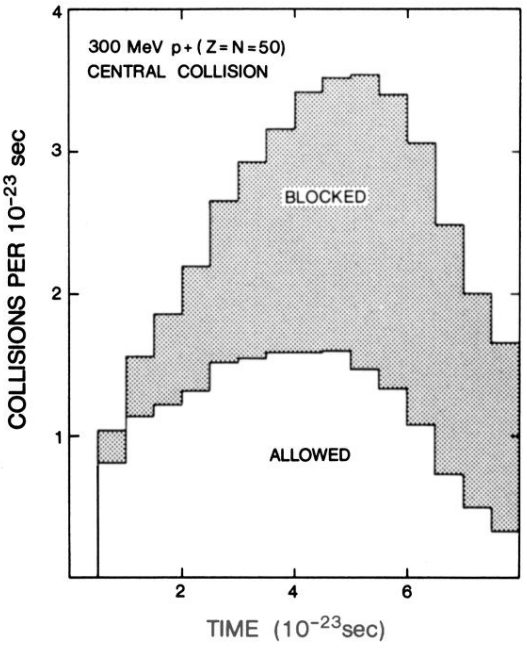

FIG. 5. Time dependence of the NN collision rate predicted for a central 300 MeV p+($N=Z=50$) reaction. Collisions solely among target nucleons in the Fermi sea are neglected. Those collisions which are Pauli-blocked are indicated by the shaded region.